Title

Universal Relationship between Conductivity and Solvation-Site Connectivity in Ether-Based Polymer Electrolytes

Journal

Macromolecules, 49(14)

ISSN

0024-9297

Authors

Pesko, Danielle M
Webb, Michael A
Jung, Yukyung
et al.

Publication Date

2016-07-26

DOI

10.1021/acs.macromol.6b00851

Peer reviewed

Macromolecules

Article

pubs.acs.org/Macromolecules

Universal Relationship between Conductivity and Solvation-Site Connectivity in Ether-Based Polymer Electrolytes

Danielle M. Pesko,[†] Michael A. Webb,[‡] Yukyung Jung,[§] Qi Zheng,[§] Thomas F. Miller, III,*[,‡] Geoffrey W. Coates,*[,§] and Nitash P. Balsara*[,†,∥,⊥]

[†]Department of Chemical and Biomolecular Engineering, University of California, Berkeley, Berkeley, California 94720, United States
[‡]Division of Chemistry and Chemical Engineering, California Institute of Technology, Pasadena, California 91125, United States
[§]Department of Chemistry and Chemical Biology, Baker Laboratory, Cornell University, Ithaca, New York 14853, United States
[∥]Materials Science Division and [⊥]Environmental Energy Technology Division, Lawrence Berkeley National Laboratory, Berkeley, California 94720, United States

Supporting Information

ABSTRACT: We perform a joint experimental and computational study of ion transport properties in a systematic set of linear polyethers synthesized via acyclic diene metathesis (ADMET) polymerization. We measure ionic conductivity, σ, and glass transition temperature, T_g, in mixtures of polymer and lithium bis(trifluoromethanesulfonyl)imide (LiTFSI) salt. While T_g is known to be an important factor in the ionic conductivity of polymer electrolytes, recent work indicates that the number and proximity of lithium ion solvation sites in the polymer also play an important role, but this effect has yet to be systematically investigated. Here, adding aliphatic linkers to a poly(ethylene oxide) (PEO) backbone lowers T_g and dilutes the polar groups; both factors influence ionic conductivity. To isolate these effects, we introduce a two-step normalization scheme. In the first step, Vogel−Tammann−Fulcher (VTF) fits are used to calculate a temperature-dependent reduced conductivity, $\sigma_r(T)$, which is defined as the conductivity of the electrolyte at a fixed value of $T - T_g$. In the second step, we compute a nondimensional parameter f_{exp}, defined as the ratio of the reduced molar conductivity of the electrolyte of interest to that of a reference polymer (PEO) at a fixed salt concentration. We find that f_{exp} depends only on oxygen mole fraction, x_0, and is to a good approximation independent of temperature and salt concentration. Molecular dynamics simulations are performed on neat polymers to quantify the occurrences of motifs that are similar to those obtained in the vicinity of isolated lithium ions. We show that f_{exp} is a linear function of the simulation-derived metric of connectivity between solvation sites. From the relationship between σ_r and f_{exp} we derive a universal equation that can be used to predict the conductivity of ether-based polymer electrolytes at any salt concentration and temperature.

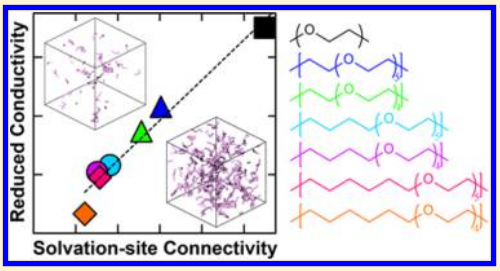

INTRODUCTION

As the size and energy density of rechargeable lithium batteries continue to be pushed to the limit, the safety of the technology is of growing concern.[1,2] Solvent-free polymer electrolytes (SPEs) are of considerable interest as they offer improved thermal stability and reduced flammability compared to that of conventional organic solvent electrolytes.[3,4] The vast majority of research in the field of SPEs has focused on polyethers such as poly(ethylene oxide) (PEO),[5−8] which form stable complexes with alkali metal ions such as Li^+.[9−11] Amorphous mixtures of PEO and lithium salts exhibit reasonable ionic conductivities on the order of 10^{-3} S/cm at 90 °C.

Substantial effort has been directed toward improving the conductivity of PEO through the incorporation of nanoparticles,[12−15] plasticizers,[16−22] or a second polymer blended into the PEO matrix.[21,23,24] Alternative approaches involve altering the chemical structure of PEO by adding cross-links,[25−27] changing the monomer chemistry,[28−30] incorporating comonomers into the PEO backbone,[31−33] and modifying the architecture of the polymer chain.[27,34−36] However, these materials have not resulted in significant improvement of electrolyte performance or commercial impact, due in part to limited understanding of the molecular mechanisms underpinning ion transport.

We recently identified that the addition of groups that do not interact with the lithium ion can dilute and alter the sites in which a lithium ion can be solvated, leading to overall reductions in ionic conductivity.[37,38] For a set of polyesters, the significantly higher conductivity of PEO relative to that of a set of polyesters was explained using the concept of solvation-site *connectivity*, quantified using molecular simulation by the number and proximity of solvation sites in the polymer matrix.[37] For a series of polyethers, a low density of solvation sites resulted in slow rates of lithium ion hopping.[38] The role of

Received: April 23, 2016
Revised: July 4, 2016
Published: July 15, 2016

DOI: 10.1021/acs.macromol.6b00851
Macromolecules 2016, 49, 5244−5255

spacing between coordinating centers has also been alluded to recently in the context of poly(ether−thioethers).[39]

In this work, we use experiments and simulations to quantify the relationship between conductivity and solvation-site connectivity in a set of polyethers in which ethylene oxide (EO) segments are regularly interrupted with carbon linkers of varying lengths (Figure 1). The polymers, labeled as C_xEO_y, are

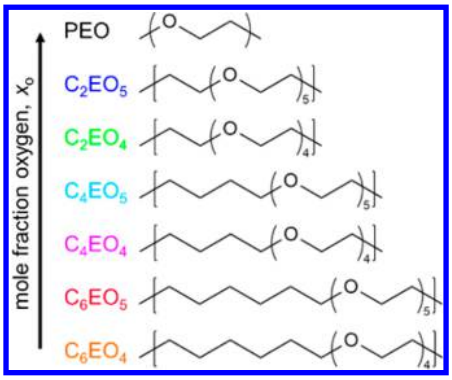

Figure 1. Structure of the C_xEO_y polyethers synthesized and characterized in this study. The naming convention specifies *x*, the length of the carbon linker, and *y*, the number of consecutive EO monomers on each segment.

distinguished by *x*, the number of carbon atoms in the carbon linker, and *y*, the number of consecutive EO monomers in the PEO segment. We show that the conductivity of C_xEO_y electrolytes can be calculated using the known conductivity of PEO electrolytes and a multiplicative correction factor that depends only on oxygen mole fraction. The same correction factor applies to the entire set of electrolytes, irrespective of temperature and salt concentration. Simulations show that introducing carbon linkers of varying lengths and frequencies affects solvation-site connectivity. The experimentally determined correction factor is shown to arise due to this connectivity.

EXPERIMENTAL AND SIMULATION METHODS

Polymer Synthesis and Characterization. We synthesized the polyethers shown in Figure 1 via acyclic diene metathesis (ADMET) polymerization,[33] followed by hydrogenation with Crabtree's catalyst (Figure 2). The diene-terminated monomers were synthesized in one step from the facile substitution reaction of the commercially available poly(ethylene glycol) (PEG) oligomers (tri- or tetraethylene glycol) with allyl bromide and 5-bromo-1-pentene to yield the C_2EO_y and C_6EO_y monomers, respectively. The C_4EO_y monomers were synthesized by mesylating PEG oligomers first and subsequently reacting with 3-butene-1-ol. This alternative procedure was used because the elimination reaction between PEG oligomers and 4-bromo-1-butene significantly lowered the yields of the desired product. The C_xEO_y monomers were then polymerized with Grubbs' first-generation catalyst. The Grubbs' catalyst was used because of its high functional group tolerance and reduced propensity for olefin isomerization reactions.[40] The synthesized unsaturated polyethers were hydrogenated using Crabtree's catalyst to yield the saturated polyethers for this study.

The C_xEO_y polymers synthesized in this study are characterized with gel permeation chromatography (GPC) for the number-averaged molecular weight (M_n) and polydispersity index ($Đ$). Thermal properties of the C_xEO_y polymers are measured with differential scanning calorimetry. The results are summarized in Table 1, along with the properties of PEO, which was commercially purchased from Polymer Source. The M_ns of the polymers range between 4.7 and 19.0 kDa (Table 1); in this range we expect ionic conductivity to be

Table 1. Properties of C_xEO_y Polymers and Poly(ethylene oxide) (PEO)

polymer[a]	M_n (kg/mol)	$Đ$	T_g (°C)	T_m (°C)	ΔH_f (J/g)	x_0
PEO	5.0	1.1	−60.0[c]	60.0[c]	193.0[c]	0.333
C_2EO_4	7.4	1.3	−72.8	−2.8	98.6	0.286
C_2EO_5	6.7	1.5	−67.0	−4.5, 9.0	16.6, 18.4	0.294
C_4EO_4	4.7	1.4	n.d.[b]	13.4	118.4	0.250
C_4EO_5	7.1	1.6	n.d.[b]	8.0	132.9	0.263
C_6EO_4	12.9	1.8	n.d.[b]	24.7, 33.4	144.2, 170.7	0.222
C_6EO_5	19.0	1.8	n.d.[b]	23.4	115.3	0.238

[a]See SI-1 for synthesis details. [b]n.d. = not detected. [c]The DSC and conductivity measurements are performed on 4.6 and 5.0 kg/mol PEO, respectively.

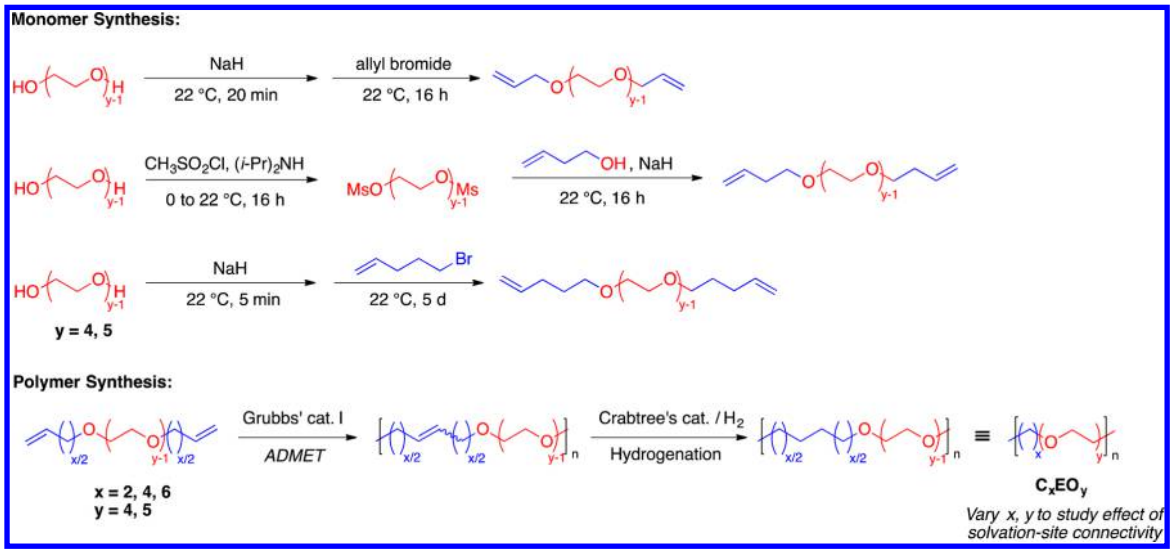

Figure 2. Synthesis of C_xEO_y monomers and polymers via acyclic diene metathesis (ADMET) polymerization followed by hydrogenation.

DOI: 10.1021/acs.macromol.6b00851
Macromolecules 2016, 49, 5244−5255

independent of M_n.[41] The reactivity of the monomers showed some dependence on the number of carbons in the linker with the longest linker (C_6) yielding the polymer with highest M_n. This trend is consistent with the literature on ADMET polymerization of oxygen-containing dienes using Schrock-type catalysts.[42,43] The glass transition temperatures, T_g, of C_2EO_4 (−72.8 °C) and C_2EO_5 (−67.0 °C) are lower than that of PEO (−60.0 °C) likely due to the increased chain flexibility of the carbon linkers. The level of crystallinity in the neat C_4EO_y and C_6EO_y precluded the observation of a T_g, but we expect that those values would decrease as the linker length increases. All of the C_xEO_y polyethers synthesized have a significantly lower T_m relative to PEO.

The mole fraction of oxygen, x_0, in each polymer is calculated according to eq 1:

$$x_0 = \frac{\text{oxygen atoms in repeat unit}}{\text{total atoms in repeat unit}} \quad (1)$$

The number of atoms in the repeat unit excludes hydrogen atoms. Values for x_0 for each polymer are shown in Table 1.

Experimental Characterization. Electrolyte preparation is performed inside of an argon glovebox (MBraun) in order to maintain water and oxygen levels below 1 and 10 ppm, respectively. The polyethers synthesized in this study, along with PEO, are dried under vacuum at 90 °C for 12 h prior to entering the glovebox. Mixtures of polymer and lithium bis(trifluoromethanesulfonyl)imide (LiTFSI) salt (Novalyte) are dissolved in anhydrous dimethylformamide (DMF) and stirred at 90 °C for a minimum of 3 h to form a homogeneous solution. The DMF is then evaporated from the solution, and the polymer/salt mixture is transferred to the glovebox antechamber and dried under vacuum for 8 h at 90 °C to remove any excess solvent. Electrolytes are prepared at varying salt concentrations, ranging from r = 0.06 to r = 0.14, where $r = [Li^+]/[O]$ is the molar ratio of lithium ions to ether oxygens. Electrolytes for C_4EO_5, C_4EO_4, and C_6EO_5 at r = 0.14 were not prepared due to limited material.

Stainless steel symmetric cells are prepared for ionic conductivity measurements of electrolytes using ac impedance spectroscopy. Samples are made by pressing the polymer electrolyte into a 254 μm thick silicone spacer and sandwiching between two 200 μm stainless steel electrodes. With the exception of crystalline PEO, all electrolytes are in the form of highly viscous liquids and are soft enough to be pressed at room temperature. The silicone forms a good seal with stainless steel, thereby preventing the electrolytes from leaking out of the cell during characterization. A micrometer is used to obtain the thickness of the electrolyte by measuring thickness of the cell and subtracting the thickness of the electrodes. Aluminum tabs are secured to the electrodes to serve as electrical contacts. The assembly is vacuum sealed in a laminated aluminum pouch material (Showa-Denko) before removing from the glovebox for electrochemical characterization.

All reported conductivity results are based on ac impedance spectroscopy performed with a Biologic VMP3 potentiostat which acquires complex impedance measurements for a frequency range of 1 Hz−1 MHz at an amplitude of 80 mV. The low-frequency minimum on the Nyquist impedance plot is taken to be the electrolyte resistance, R, which is used along with electrolyte thickness, l, and electrolyte area, a, to calculate the electrolyte conductivity, σ, according to eq 2:

$$\sigma = \frac{l}{aR_b} \quad (2)$$

The inner diameter of the spacer, 3.175 mm, is used to calculate a. Thickness, l, is taken to be the final thickness of the electrolyte, measured after conductivity measurements are completed. On average, the electrolyte thickness decreased 3.5% after annealing. The symmetric cells are disassembled to allow for visual inspection of the electrolyte. Any samples that exhibited bubbles or voids in the polymer are discarded from the set, as such defects would alter the electrolyte volume and produce inaccurate conductivity results. Fewer than 5% of samples prepared in this study exhibited such characteristics. The conductivity for each electrolyte is determined by averaging the results from three different samples, and the error bars signify the standard deviation of these measurements. The conductivity of the neat polymer is subtracted from that of the salt-containing electrolytes to account for ionic impurities that may be present. The conductivity at r = 0 at 90 °C was below 10^{-5} S/cm for all of the polymers in this study.

DSC experiments are performed on a TA Instruments DSC Q200 instrument to obtain the T_g and T_m of each electrolyte. DSC samples are prepared inside of the glovebox, where aluminum pans are filled with 1−5 mg of electrolyte and hermetically sealed before removing from the glovebox. The following protocol is used for the temperature scan: heat to 110 °C at 20 °C/min, cool to −90 °C at 5 °C/min, and heat to 110 °C at 20 °C/min. Values for T_g and T_m are obtained from the second heating scan. DSC measurements are repeatable within 1.0 °C.

Molecular Dynamics Simulations. All MD simulations employ a united atom force field, with bonding parameters taken from CHARMM[44] and all other parameters taken from the TraPPE-UA force field;[45] compatible lithium ion parameters are obtained from a previous simulation study.[46] Force field parameters used in this study are provided in SI-2. All simulations are performed using the LAMMPS simulation package[47] with GPU acceleration.[48,49] The equations of motion are evolved using the velocity-Verlet integrator with a 1 fs time step. Particle−particle−particle mesh Ewald summation[48] is used to compute all nonbonded interactions beyond a 14 Å cutoff. The Nosé−Hoover (100 fs relaxation) and Nosé−Hoover barostat (1000 fs relaxation) are used in all simulations to control the temperature and pressure.

Two sets of simulations are performed for the C_xEO_y polymers. For polymers with x = 2, 4, and 6 and y = 3−8, neat-polymer simulations are used to obtain polymer properties and solvation-site connectivity metrics. For polymers with x = 2 and y = 3−8, simulations of a single lithium cation diffusing in a polymer are used to investigate the lithium ion solvation environment.

For the neat-polymer simulations, four independent copies of the simulation cell are generated for each polymer studied. Each copy consists of a single, long polymer chain ($M_n \sim 25$ kg/mol) with an initial configuration generated via a self-avoiding random walk. For the ion-containing simulations, the same procedure is used, except that a single lithium cation is randomly placed in the simulation cell, and the total charge of the system is neutralized with a uniform background charge.[50] To generate starting configurations for MD production runs, the systems are equilibrated in five steps. In step 1, the initial configuration is relaxed for 10 000 steps with nonperiodic boundary conditions using steepest descent energy minimization with the maximum atom displacement limited to 0.1 Å for any given step. In step 2, the system is annealed at 726.85 °C with periodic boundary conditions using 100 000 steps of Langevin dynamics with a 100 fs damping factor. In step 3, the simulation cell is adjusted at a constant rate over 500 ps at 226.85 °C to achieve a cubic simulation cell with a density of 1.0 g/cm^3. In step 4, the system is annealed for 1.5 ns at 226.85 °C and 1 atm. In step 5, the system is equilibrated for 10 ns at 90 °C and 1 atm. A similar protocol was employed in ref 38.

Following equilibration, production runs of 10 ns for the neat-polymer simulations and of 150 ns for the ion-containing systems are performed at 90 °C and 1 atm.

RESULTS AND DISCUSSION

Experimental Characterization. The ionic conductivity, σ, of the C_xEO_y polyethers and PEO was measured as a function of temperature, T, in the range of 27−110 °C. Figure 3 shows the results at a fixed salt concentration, r = 0.08, which is in the vicinity where PEO conductivity is maximized.[5] Results from Figure 3 indicate that the σ of the C_xEO_y polyethers are within 1 order of magnitude of PEO at all temperatures. The relative ordering of the polymers does not change significantly as T is varied. We observe that at any given T C_2EO_5 and PEO exhibit the highest σ, which are comparable within error. Of the

DOI: 10.1021/acs.macromol.6b00851
Macromolecules 2016, 49, 5244−5255

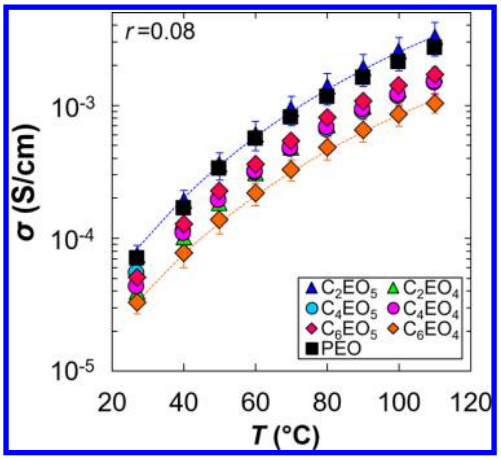

Figure 3. Conductivity, σ, with increasing temperature at r = 0.08.

polyethers synthesized in this study, C_2EO_5 has the shortest carbon linker (two) and the longest consecutive segment of ethylene oxide (EO) monomers (five); thus, C_2EO_5 has the largest mole fraction of oxygen, x_0 (Table 1), of the C_xEO_y polymers. Similarly, C_6EO_4 has the lowest x_0 and exhibits the lowest σ. As one might anticipate, results from Figure 3 suggest that there is a relationship between the x_0 and σ.

To further explore this relationship, in Figure 4a we plot σ of the C_xEO_y polyethers and PEO as a function of x_0 at r = 0.08 and 90 °C. The measured conductivities of the polymers are within a narrow range between 6.5×10^{-4} and 1.7×10^{-3} S/cm. In some cases increasing the linker length increases σ (C_2EO_4 vs C_4EO_4), while in other cases it decreases σ (C_2EO_5 vs C_4EO_5). Similarly, an additional consecutive EO unit in the monomer may either increase σ (C_2EO_4 vs C_4EO_5) or decrease σ (C_4EO_4 vs C_4EO_5). The lack of clear trends in this data most likely results from two competing effects upon the addition of carbon linkers. Namely, the presence of the linkers dilutes the density of lithium ion solvation sites (making hopping between sites less probable) but simultaneously changes the thermal properties of the polymer melt. Figure 4b shows the glass transition temperature, T_g, of the C_xEO_y and PEO electrolytes at a salt concentration of r = 0.08. It is evident that decreasing x_0 decreases T_g due to increased chain flexibility. It is generally accepted that more flexible chains promote ion transport due to rapid segmental motion.[8,51−54]

In an attempt to decouple the effects of solvation-site density and segmental motion, we calculate a reduced conductivity, σ_r. Similar approaches have been used previously in analysis of experimental data from polymer electrolytes.[5,55−57] To calculate σ_r, we use a modified Vogel−Tammann−Fulcher (VTF) equation where the temperature is defined to be a fixed distance (75 K) above the measured T_g of the electrolyte:

$$\sigma_r = A(T_g + 75\ \mathrm{K})^{-1/2} \exp\left(\frac{-E_a}{R(125\ \mathrm{K})}\right) \quad (3)$$

The two dotted curves in Figure 3 show VTF fits for C_2EO_5 and C_6EO_4 (other fits are omitted for clarity). These fits enable estimation of a pseudoactivation energy, E_a, and a prefactor, A. Figure 4c shows σ_r of the C_xEO_y polyethers and PEO as a function of x_0. Once the contribution from T_g differences is corrected for it becomes clear that the reduced conductivity is a monotonically increasing function of x_0. In other words, decreasing the linker length or the addition of an EO unit leads

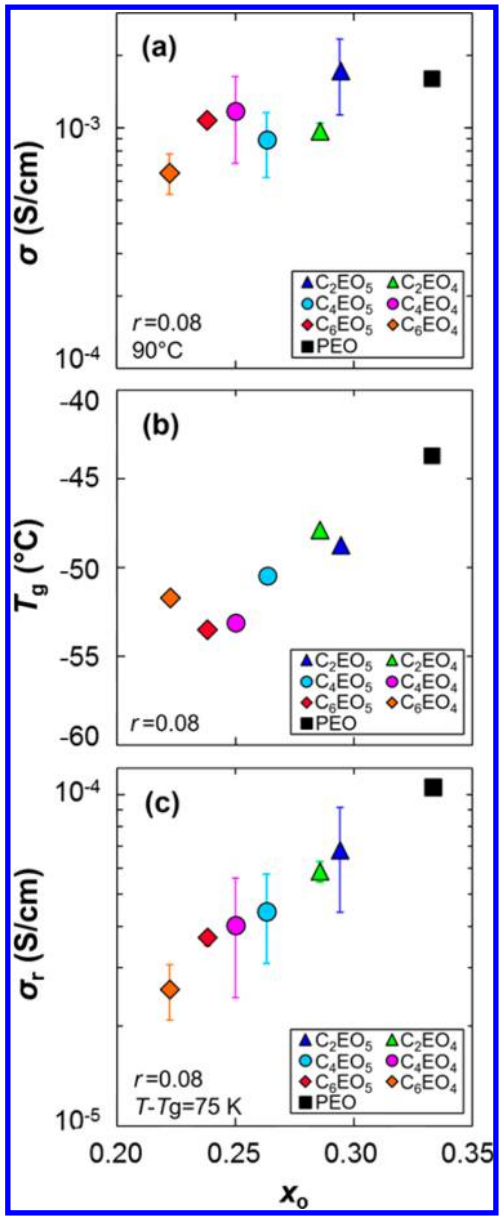

Figure 4. (a) Conductivity, σ, at 90 °C, (b) glass transition temperature, T_g, and (c) reduced conductivity, σ_r, with increasing mole fraction of oxygen atoms, x_0, on the polymer backbone. All data are collected at a salt concentration of r = 0.08.

to an increase in σ_r. Since the VTF curves for the polymers are essentially parallel, the dependence of σ_r on x_0 is qualitatively similar to that seen in Figure 4c at all values of $T - T_g$. All of the electrolytes in Figure 4c have a fixed salt concentration of r = 0.08; as $r = [Li^+]/[O]$, electrolytes with a lower x_0 value will typically have fewer salt molecules per unit volume. Consequently, it is unclear whether the trend observed in Figure 4c is due to changes in molecular structure or simply results from changes in volumetric density of charge carriers in the electrolytes.

To isolate the effect of monomer structure on conductivity, we define a new variable that we call the experimental connectivity, f_{exp}:

DOI: 10.1021/acs.macromol.6b00851
Macromolecules 2016, 49, 5244−5255

$$f_{exp} = \left(\frac{\sigma_r}{\sigma_{r,PEO}}\right)_{r,T-T_g} \left(\frac{x_{0,PEO}}{x_0}\right) \quad (4)$$

The ratio of $\sigma_r / \sigma_{r,PEO}$ at a given r and $T - T_g$ quantifies the conductivity of a C_xEO_y electrolyte relative to that of PEO, correcting for the different T_g values of the C_xEO_y electrolyte. The ratio of $x_{0,PEO}/x_0$ represents the ratio of the moles of salt in a C_xEO_y electrolyte relative to that of PEO, given that $r = [Li^+]/[O]$, approximately correcting for differences in the volumetric density of salt (see the SI-3). The use of mole fractions in eq 4 requires two main assumtions: (1) the salt does not contribute to the overall volume, and (2) all atom moieties (i.e., O or CH_2) have the same partial molar volume. Equation 4 is similar to the expression for conductivity in block copolymer systems where a morphology factor is used to describe the constraints on ion transport imposed by the geometry of the conducting phase.[58−60] The strategy is also somewhat similar to work that compared conductivities of liquid electrolytes at the same dielectric constant,[61] but here we compare conductivities in ether-based polymer electrolytes at the same r and $T - T_g$.

Figure 5 is a plot of f_{exp} versus x_0. This plot shows that f_{exp} increases monotonically with increasing x_0. Since other effects have been factored out, the change in f_{exp} with x_0 is attributed to changes in the local environment of the lithium ion. As x_0 is decreased, there are likely more carbon linker segments and fewer EO segments in the vicinity of each solvated lithium ion. Assuming the carbon linkers are ionically insulating, polymers with a lower x_0 are expected to exhibit slower lithium ion diffusion, as it takes longer for the ion to hop to an adjacent solvation site. Thus, f_{exp}, is an experimentally determined quantity that is expected to report on the proximity of lithium ion solvation sites.

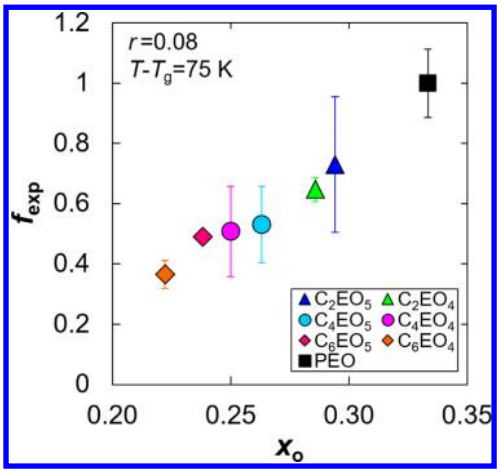

Figure 5. Experimental connectivity, f_{exp}, with increasing x_0 at $r = 0.08$ and $T - T_g = 75$ K.

In Figure 6a, we plot f_{exp} versus x_0 at $r = 0.08$ and different reduced temperatures. We find that there is a linear relationship between f_{exp} versus x_0 that is to a good approximation, independent of $T - T_g$. To investigate the behavior of f_{exp} across different salt concentrations, the analysis was repeated at different values of r, and the results for f_{exp} values are shown in Figure 6b. Data for σ, T_g, and σ_r at all salt concentrations used to obtain the f_{exp} values in Figure 6b are provided in SI-4. In Figure 6c we show results for f_{exp} at all values of r at different reduced temperatures. All data in Figure 6 are consistent with a line

$$f_{exp} = 5.39x_0 - 0.86 \quad (5)$$

obtained by a linear fit of the data in Figure 6c.

Figure 6 provides justification for the normalization scheme used in this study. It is evident from Figure 6 that when polymer electrolytes are compared using σ_r and differences in the volumetric density of salt are factored out using x_0, ion transport is related to a parameter (f_{exp}) that is largely independent of temperature and salt concentration. It appears as though f_{exp} is an intrinsic property of the neat polymer in the absence of salt.

Molecular Dynamics Simulations. We now use MD simulations to further understand how varying the composition of the C_xEO_y polymers affects lithium ion solvation and polymer properties, including the connectivity between possible lithium ion solvation sites.

Figure 7 presents an analysis of the lithium ion solvation environments observed during MD simulations of the C_2EO_y polymers in the presence of an isolated lithium ion. Representative snapshots of the lithium ion solvation shell are shown in Figure 7a. In all cases, the lithium ion coordinates with one or two contiguous sequences of oxygen atoms, which is similar to coordination environments previously observed in PEO.[8,37,62] While complexation by a single contiguous sequence of oxygen atoms is expected to be difficult in the presence of carbon linkers, the snapshots for C_2EO_3 and C_2EO_4 depict configurations for which the lithium cation indeed coordinates with oxygen atoms separated by a linker. In general, the snapshots display strikingly similar solvation environments in terms of the number of coordinating oxygen atoms despite the changing frequency of the C_2 linker. This is confirmed in Figure 7b, which shows the lithium−oxygen cumulative distribution function (CDF), and in Figure 7c, which presents the frequency with which different lithium ion binding motifs are observed in the simulations. Both Figure 7b and Figure 7c indicate that lithium ions in the C_2EO_y polymers are coordinated by five or six oxygen atoms, irrespective of the number consecutive EO units; similar findings are anticipated for the C_4 and C_6 linkers based on previous simulation studies.[37,38]

We now focus on neat-polymer simulations, i.e., in the absence of the lithium ion, to examine how the addition of carbon linkers affects both the thermal properties of the polymer and the distribution of lithium ion solvation sites. Figure 8 compares these two properties obtained for the expanded set of polymers (C_xEO_y for $x = 2$, 4, and 6 and $y = 3$−8). Figure 8a shows that the bulk modulus, B, at 90 °C for the polymers generally increases with increasing x_0. The polymers with C_2 linkers have larger bulk moduli than those with C_4 and C_6 linkers, and PEO (black square) possesses the largest bulk modulus among all the polymers characterized. These results are qualitatively consistent with the experimental observations in Figure 4b that the T_g of the electrolytes generally increases with x_0 and decreases with increasing linker length.

In contrast to Figure 8a, Figure 8b shows that the average nearest-neighbor distance, $\langle r_{nn} \rangle$, between lithium ion solvation sites generally decreases with increasing x_0. Here, a solvation site is defined at the centroid of a set of five or more oxygen atoms if each oxygen is also within 3.5 Å of the centroid; two sites are combined if the distance between their centroids is less

DOI: 10.1021/acs.macromol.6b00851
Macromolecules 2016, 49, 5244−5255

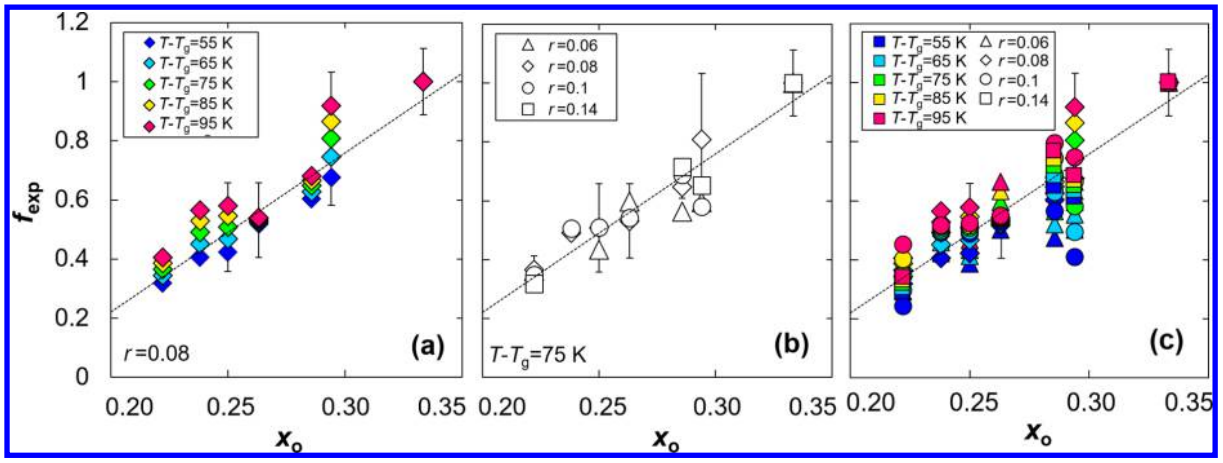

Figure 6. Experimental connectivity, f_{exp}, with increasing x_0 at varying (a) $T - T_g$, (b) r, and (c) $T - T_g$ and r. The green diamonds in (a) and (c) and the white diamonds in (b) show the data from Figure 5 with r = 0.08 and $T - T_g$ = 75 K; error bars are only shown for this set of data. The dashed line is the same in all three figures and represents the best linear fit of the data in (c), given by eq 5. The correlation coefficients for the linear fits are 0.87, 0.90, and 0.85 for (a–c), respectively.

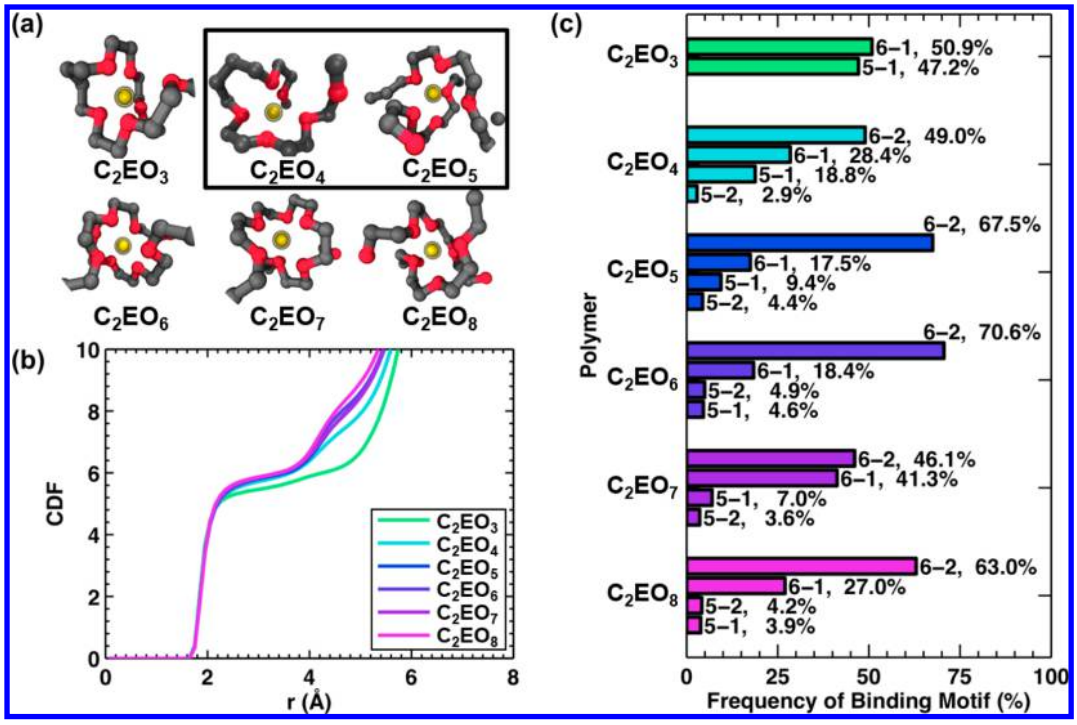

Figure 7. Analysis of the lithium ion solvation environment for polymers with C_2 linkers between EO repeat units. (a) Simulation snapshots of representative lithium ion solvation structures in polymers with different numbers of repeating EO units. The boxed snapshots correspond to polymers that have experimental data. (b) The cumulative number of oxygen atoms as a function of distance from the lithium ion, given by the lithium–oxygen cumulative distribution function (CDF). (c) Frequency of occurrence of observed lithium ion binding motifs. The first number indicates the number of oxygen atoms that are within 3.25 Å of the lithium ion; the number after the dash refers to the number of different contiguous polymer chain segments.

than r_{min} = 1 Å. The figure shows that modifying the number of contiguous EO units and the length of the linker directly influences the number and proximity of solvation sites. Notably, PEO has the shortest average distance between neighboring lithium ion solvation sites. Figures 8a and 8b combine to highlight a difficulty in designing polymers with enhanced cation diffusivity since increasing the number and proximity of lithium ion solvation sites often increases polymer stiffness, in accordance with the experimental observations in Figure 4a.

Previous work introduced solvation-site connectivity as an intuitive means of explaining trends in conductivity.[37] To examine this effect for the C_xEO_y polymers, Figure 9 compares the distribution and proximity of solvation sites for PEO, which is the most conductive polymer in Figure 4c, and C_6EO_4, which is the least conductive. Figures 9a and 9d depict representative snapshots of the neat PEO and C_6EO_4 melts, respectively. Solvation sites in these snapshots are depicted as blue spheres in Figures 9b (PEO) and 9e (C_6EO_4). Figures 9c and 9f depict edges connecting the solvation sites within a cutoff distance, r_{cut} = 3 Å. Comparing Figures 9b and 9e reveals that introduction of the C_6 linker decreases the density of solvation sites in the polymer. Moreover, comparing Figures 9c and 9f illustrates that

DOI: 10.1021/acs.macromol.6b00851
Macromolecules 2016, 49, 5244–5255

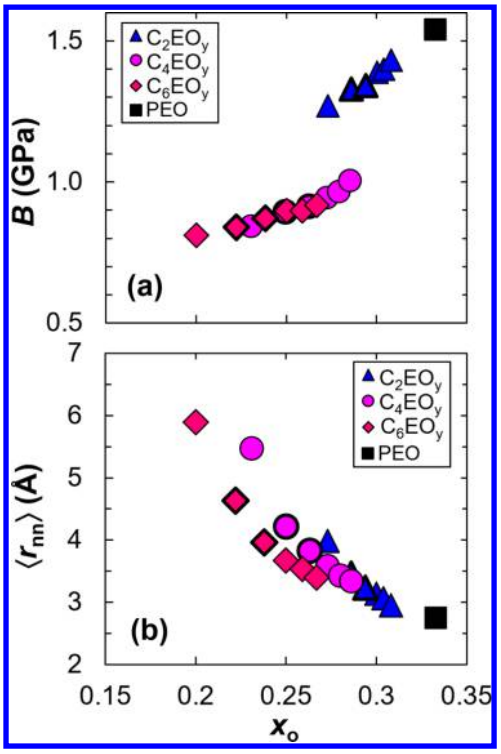

Figure 8. Variation of (a) the polymer bulk modulus, B, at 90 °C and (b) the average nearest-neighbor separation distance between solvation sites, $\langle r_{nn} \rangle$, as a function of x_0 for polymers with different linkers. In both (a) and (b), polymers with different linkers are denoted by different symbols. Markers with bold outlines indicate polymers that were also experimentally characterized.

C_6EO_4 has far fewer edges than PEO. Because hopping among solvation sites is a primary mode of lithium ion transport and hopping is typically limited to distances less than 3 Å,[8,38] having fewer edges between solvation sites is expected to reduce the overall rate of lithium ion diffusion.

From Figures 6, 8b, and 9, it is clear that x_0 plays an important role in both the solvation-site connectivity and f_{exp}. To further establish the relationship between solvation-site connectivity and f_{exp}, we examine three possible metrics for characterizing the solvation-site connectivity from the simulations, including κ (the volumetric density of edges between solvation sites), λ (the linear density of edges projected along a given linear direction), and $\exp[-\langle r_{nn} \rangle]$ (a proportionality to a characteristic hopping rate). Figure 10 provides a visual representation of these metrics for PEO. The first metric, κ (Figure 10a), is computed using

$$\kappa = \frac{1}{V} \sum_{i<j} H(r_{cut} - r_{ij}) \tag{6}$$

where V is the volume of the simulation cell, the summations run over pairs of solvation sites in the simulation cell, and $H(r)$ is the typical Heaviside step function. Similarly, the second metric, λ (also shown in Figure 10a), is computed using

$$\lambda = \frac{1}{L_u} \sum_{i<j} H(r_{cut} - \sqrt{\mathbf{r}_{ij} \cdot \mathbf{u}}) \tag{7}$$

where L_u is the length of a given linear dimension in the simulation cell, $\mathbf{u}$ is a unit vector in the direction of that linear dimension, and $\sqrt{\mathbf{r}_{ij} \cdot \mathbf{u}}$ is the magnitude of the distance vector $\mathbf{r}_{ij}$ projected onto $\mathbf{u}$. The third metric, $\exp[-\langle r_{nn} \rangle]$ (Figure 10b), is expected to be proportional to a characteristic hopping rate

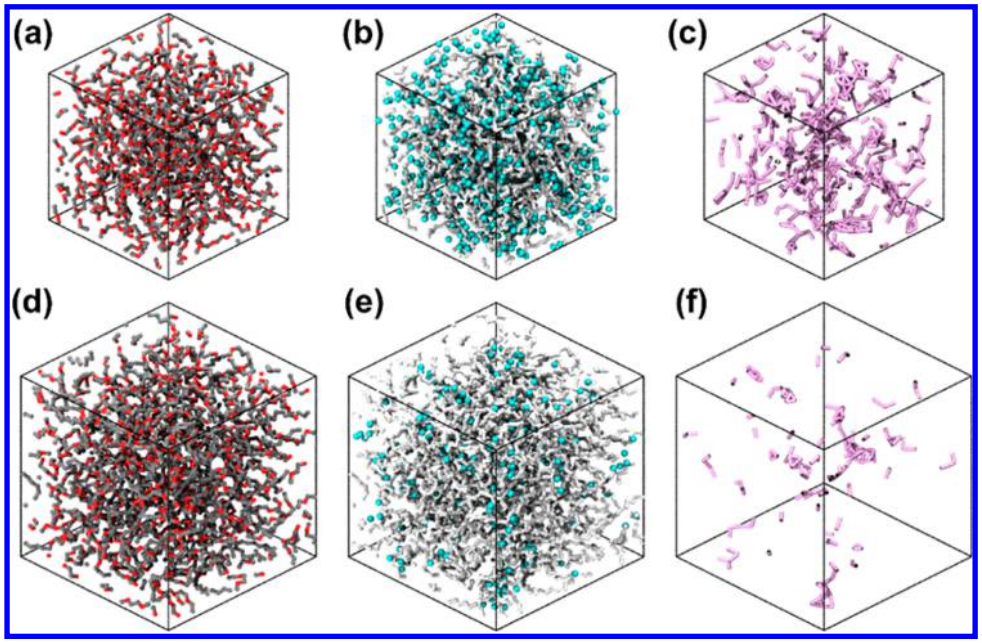

Figure 9. Comparison between simulation snapshots for (a–c) PEO and (d–f) C_6EO_4 showing (a, d) a representative configuration of the neat polymer melt, (b, e) possible lithium ion solvation sites within the melt, and (c, f) edges less than 3 Å in length between the solvation sites in (b, e). In (a, d) carbon atoms are gray, and oxygen atoms are red. In (b, e), all polymer atoms are light gray while the solvation sites are depicted as blue spheres. In (c, f), edges between solvation sites are depicted as purple bonds while the polymer is not shown for clarity. The various simulation snapshots have the same size scale; the difference in size between the simulation box for PEO and that of C_6EO_4 is due to the latter having a larger number of atoms and a lower density.

DOI: 10.1021/acs.macromol.6b00851
Macromolecules 2016, 49, 5244–5255

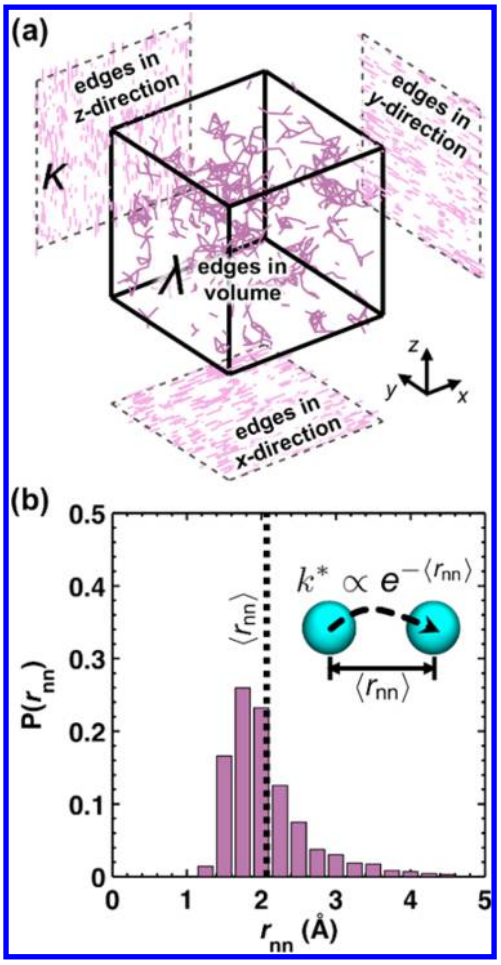

Figure 10. Relationship between connectivity metrics in PEO. (a) Edges between solvation sites in the simulation cell, which defines the volumetric edge density κ, and projections of the edges in the x-, y-, and z-directions, which define the linear edge density λ. (b) Distribution of nearest-neighbor separation distances, which defines the average nearest-neighbor separation distance $\langle r_{nn}\rangle$ used to compute a characteristic hopping rate $\exp[-\langle r_{nn}\rangle]$.

between solvation sites separate by $\langle r_{nn}\rangle$, which is computed using

$$\langle r_{nn}\rangle = \frac{1}{N}\sum_i \min_{j>i}[r_{ij}] \tag{8}$$

where N denotes the number of solvation sites in the simulation cell. All three quantities are likely to increase if the number of sites increases or the distance between solvation sites decreases, and so each reasonably reports on the concept of connectivity.

Figure 11 presents the dependence of all three metrics for characterizing the connectivity on x_0. All of the metrics, which are normalized with respect to PEO, increase with increasing x_0 for a given linker. This is sensible because the number of consecutive EO units is increasing, making lithium ion solvation sites more prevalent. It is interesting to note that polymers with C_6 linkers are characterized by higher connectivity than polymers with C_4 or C_2 linkers when the oxygen mole fraction is comparable, up to $x_0 = 0.27$. This is likely because the C_6EO_y polymers require more contiguous EO units to achieve the same oxygen mole fractions as the polymers with shorter linkers.

Comparison of Experiment and Simulations. Figure 12 directly examines the correlation between the experimentally calculated f_{exp} and the theoretically derived connectivity metrics. The linear fits shown in Figure 12a–c quantify the relationship between f_{exp} and connectivity. The relationships thus obtained are

$$f_{exp} = a_i + m_i C_i \quad (i = 1 - 3) \tag{9}$$

where C_i represent the three connectivity metrics ($C_1 = \kappa/\kappa_{PEO}$, $C_2 = \lambda/\lambda_{PEO}$, $C_3 = \exp[-\langle r_{nn}\rangle]/\exp[-\langle r_{nn}\rangle_{PEO}]$). The fits give ($a_1 = 0.34$, $m_1 = 0.69$), ($a_2 = 0.31$, $m_2 = 0.72$), and ($a_3 = 0.30$, $m_3 = 0.71$). To a good approximation the relationship between f_{exp} and the connectivity metrics is linear with an intercept of 0.32 and a slope of 0.71 (average values of a_i and m_i, respectively). The behavior of the ether-based electrolytes in the low C_i limit remains an interesting open question. One may expect f_{exp} to approach zero as C_i approaches zero, but the data in Figure 12 extrapolate to a finite positive value (0.32) as C_i approaches 0. One possibility is that the linear relationships in Figure 12 breaks down at $0 < C_i < 0.15$, perhaps due to a change in ion hopping mechanism in the low connectivity limit ($C_i < 0.15$) or due to the neglect of anion transport or ion–ion

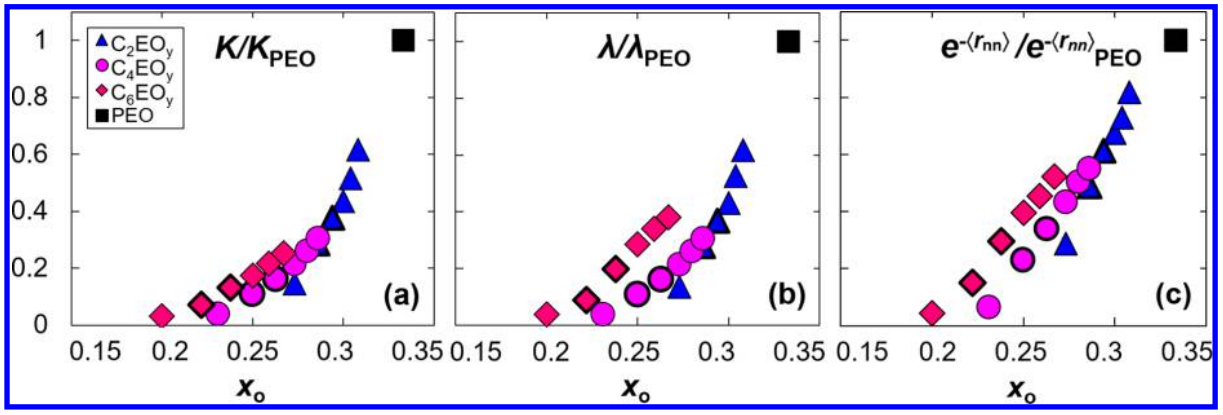

Figure 11. Analysis of simulated connectivity metrics as a function of x_0 for polymers with different linkers, including (a) κ, the volumetric connectivity (number of edges between solvation sites per unit volume), (b) λ, the linear connectivity (number of edges between solvation sites per unit length), and (c) $\exp[-\langle r_{nn}\rangle]$, a characteristic distance-dependent proportionality for the lithium ion hopping rate. Each metric is normalized by the corresponding value for PEO. In all panels, polymers with different linkers are denoted by different symbols. Markers with bold outlines indicate polymers that were also experimentally characterized.

DOI: 10.1021/acs.macromol.6b00851
Macromolecules 2016, 49, 5244–5255

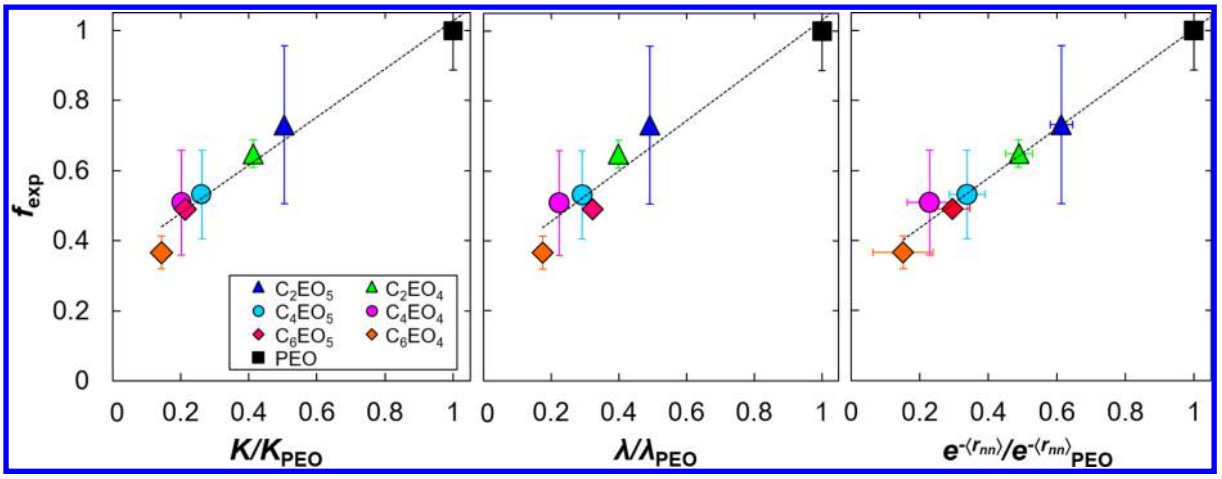

Figure 12. Correlation of experimental connectivity, f_{exp}, and the theoretical connectivity metrics in Figure 11a–c. The dashed line shows the linear fit to the data. The correlation coefficients for the linear fits are 0.91, 0.89, and 0.98 for (a–c), respectively.

interactions in our simulations. Nevertheless, Figure 12 makes clear that f_{exp}, which is obtained from analysis of experimentally measured conductivities of a series of ether-based polymer electrolytes, is strongly correlated with the solvation-site connectivity that manifests in simulations of neat polymers. For other classes of polymers, we have found that the calculated solvation-site connectivity does not necessarily correlate directly with x_0,[37] and we likewise do not expect that in general for f_{exp}; in this sense, the results in Figures 5 and 6 are likely a special feature of the class of polyethers considered here. Nonetheless, generally across polymers, we do expect a strong correlation between the experimental and calculated metrics of connectivity, as shown in Figure 12.

CONCLUSIONS

The role of polymer segmental motion and the glass transition temperature on the conductivity of polymer electrolytes has long been appreciated. When comparing polymers with different monomer chemistries, the nature and distribution of ion solvation sites may also play an important role. To investigate these effects, a combined experimental and computational study of ion transport is performed on a systematic set of polymer electrolytes in which aliphatic linkers have been added to a PEO backbone. Experiments are conducted on mixtures of the ether-based polymers and LiTFSI over a wide range of salt concentrations, while the simulations focus on the solvation of lithium ions in the dilute salt limit and the distribution of available lithium solvation sites in neat polymers.

The experimentally measured conductivities are affected by a variety of often competing factors, including T_g and also the density of available ion solvation sites. To isolate the effects of these factors, we employ a two-step normalization scheme. In the first step, VTF fits are used to calculate a temperature-dependent reduced conductivity, $\sigma_r(T - T_g)$, which is defined as the conductivity of the electrolyte at a fixed value of $T - T_g$. This step mitigates differences in the conductivity of polymers that arise due to disparities in T_g. In the second step, we compute a dimensionless parameter f_{exp}, defined as the ratio of the reduced molar conductivity of the electrolyte of interest to that of a reference polymer (PEO) at a fixed salt concentration. This parameter is used to assess to what extent changes in conductivity can be attributed to factors other than T_g, such as due to differences in the connectivity of solvation sites. Remarkably, within the set of polyethers studied, f_{exp} is shown to depend only on oxygen mole fraction, x_0, and is largely independent of temperature and salt concentration. This suggests that f_{exp} is an intrinsic property of the neat polymer that distinguishes the conductivity of polymers at a given concentration and $T - T_g$.

Molecular dynamics simulations conducted on neat polymers and polymers in the presence of an isolated lithium ion are used to develop molecular insight for f_{exp} and its dependence on x_0. The latter simulations are used to identify the nature of lithium ion solvation sites, and the distribution of such sites is examined in simulations of neat polymer systems. We introduce three metrics for quantifying the connectivity among solvation sites using simulation ($C_1 = \kappa/\kappa_{PEO}$, $C_2 = \lambda/\lambda_{PEO}$, $C_3 = \exp[-\langle r_{nn}\rangle]/\exp[-\langle r_{nn}\rangle_{PEO}]$). In the range $0.15 < x_0 < 0.33$, we find that f_{exp} is correlated with the various connectivity metrics according to $f_{exp} = 0.32 + 0.71C_i$. The simulations thus provide molecular insight into the underpinnings of f_{exp}. Namely, f_{exp} reports on the proximity of lithium ion solvation sites in the polymer, which is essential in facilitating lithium ion diffusion in polymer electrolytes.

On the basis of these analyses, we present a universal equation using $\sigma_{PEO}(r,T)$, the well-established dependence of conductivity of PEO electrolytes on salt concentration and temperature

$$\sigma(r,\ T - T_{g,PEO} + T_g) = \sigma_{PEO}(r,\ T) \times (3x_0) \times (5.39x_0 - 0.86) \quad (10)$$

where the last term is obtained by linear fit of the f_{exp} data in Figure 6. Note that T_g refers to the glass transition temperature of the polymer/salt mixture, which can be either measured or approximated using the data presented in this paper (see SI-5). The practical value of eq 10 is that the conductivity of ether-based electrolytes at salt concentrations and temperatures similar to those in this study can be easily predicted on the basis of its molecular composition. This equation highlights two approaches that may be employed for designing polymer electrolytes with improved conductivity: (1) increase f_{exp} while keeping T_g close to that of PEO or (2) decrease T_g while keeping f_{exp} close to unity.

DOI: 10.1021/acs.macromol.6b00851
Macromolecules 2016, 49, 5244–5255

■ ASSOCIATED CONTENT

Supporting Information

The Supporting Information is available free of charge on the ACS Publications website at DOI: 10.1021/acs.macromol.6b00851.

Synthesis details including monomer synthesis, polymerization procedure, and NMR spectra; force-field parameters for MD simulations; derivation of the formula used to calculate f_{exp}; experimental data for σ, T_g, and σ_r at all salt concentrations; details on how to approximate conductivity using the universal equation (PDF)

■ AUTHOR INFORMATION

Corresponding Authors

*E-mail: nbalsara@berkeley.edu (N.P.B.).
*E-mail: gc39@cornell.edu (G.W.C.).
*E-mail: tfm@caltech.edu (T.F.M.).

Author Contributions

D.M.P., M.A.W., and Y.J. contributed equally to the work.

Notes

The authors declare no competing financial interest.

■ ACKNOWLEDGMENTS

The authors gratefully acknowledge Zhen-Gang Wang for useful discussions. This research was supported by the National Science Foundation under DMREF Award NSF-CHE-1335486. DSC experiments were performed at the Molecular Foundry user facilities at Lawrence Berkeley National Laboratory supported by the Office of Science, Office of Basic Energy Sciences, of the U.S. Department of Energy under Contract DE-AC02-05CH11231. M.A.W. also acknowledges support from the Resnick Sustainability Institute

■ TERMINOLOGY

SPEs	solvent-free polymer electrolytes
PEO	poly(ethylene oxide)
PEG	poly(ethylene glycol)
EO	ethylene oxide
ADMET	acyclic diene metathesis
LiTFSI	lithium bis(trifluoromethanesulfonyl) imide
DMF	dimethylformamide
DSC	differential scanning calorimetry
VTF	Vogel−Tammann−Fulcher
CDF	cumulative distribution function
M_n	number-averaged molecular weight (kg/mol)
T_g	glass transition temperature (°C)
T_m	melting temperature (°C)
$Đ$	polydispersity
x_0	mole fraction of oxygen
r	molar ratio of Li^+ to ether oxygens
R_b	bulk electrolyte resistance (Ω)
l	electrolyte thickness (cm)
a	electrolyte area (cm^2)
σ	conductivity (S/cm)
T	temperature (°C)
σ_r	reduced conductivity (S/cm)
A	VTF prefactor (S $K^{1/2}$/cm)
E_a	effective activation energy (kJ/mol)
R	universal gas constant (kJ/(mol K))
f_{exp}	experimental connectivity
B	bulk modulus (GPa)
$\langle r_{nn} \rangle$	average nearest-neighbor distance between solvation sites (Å)
r_{min}	minimum distance for edges between solvation sites (Å)
r_{cut}	maximum distance for edges between solvation sites (Å)
κ	weighted volumetric density of edges between viable solvation sites
V	volume of the simulation cell
$w(r)$	function for weighting a particular edge based on distance
$H(r)$	Heaviside step function
λ	linear density of edges projected along a given linear direction
$\mathbf{u}$	unit vector in the direction of the linear dimension
L_u	length of a linear dimension (in the direction of $\mathbf{u}$) in the simulation cell
$\mathbf{r}_{ij}$	distance vector between sites with indices i and j
k^*	lithium ion hopping rate at $\langle r_{nn} \rangle$
C_i	generalized and normalized connectivity metric
a_i	intercept in equation relating C_i and f_{exp}
m_i	slope in equation relating C_i and f_{exp}

■ REFERENCES

(1) Scrosati, B.; Garche, J. Lithium batteries: Status, prospects and future. *J. Power Sources* **2010**, *195* (9), 2419−2430.
(2) Tarascon, J. M.; Armand, M. Issues and challenges facing rechargeable lithium batteries. *Nature* **2001**, *414* (6861), 359−367.
(3) Meyer, W. H. Polymer electrolytes for lithium-ion batteries. *Adv. Mater.* **1998**, *10* (6), 439−448.
(4) Scrosati, B.; Vincent, C. A. Polymer Electrolytes: The Key to Lithium Polymer Batteries. *MRS Bull.* **2000**, *25* (03), 28−30.
(5) Lascaud, S.; Perrier, M.; Vallee, A.; Besner, S.; Prud'homme, J.; Armand, M. Phase Diagrams and Conductivity Behavior of Poly(ethylene oxide)-Molten Salt Rubbery Electrolytes. *Macromolecules* **1994**, *27* (25), 7469−7477.
(6) Shi, J.; Vincent, C. The effect of molecular weight on cation mobility in polymer electrolytes. *Solid State Ionics* **1993**, *60* (1−3), 11−17.
(7) Gorecki, W.; Jeannin, M.; Belorizky, E.; Roux, C.; Armand, M. Physical properties of solid polymer electrolyte PEO(LiTFSI) complexes. *J. Phys.: Condens. Matter* **1995**, *7* (34), 6823−6832.
(8) Borodin, O.; Smith, G. D. Mechanism of Ion Transport in Amorphous Poly(ethylene oxide)/LiTFSI from Molecular Dynamics Simulations. *Macromolecules* **2006**, *39* (4), 1620−1629.
(9) Fenton, D. E.; Parker, J. M.; Wright, P. V. Complexes of alkali metal ions with poly(ethylene oxide). *Polymer* **1973**, *14* (11), 589.
(10) Shriver, D.; Papke, B.; Ratner, M.; Dupon, R.; Wong, T.; Brodwin, M. Structure and ion transport in polymer-salt complexes. *Solid State Ionics* **1981**, *5*, 83−88.
(11) Borodin, O.; Smith, G. D. Molecular Dynamics Simulations of Poly(ethylene oxide)/LiI Melts. 1. Structural and Conformational Properties. *Macromolecules* **1998**, *31* (23), 8396−8406.
(12) Croce, F.; Persi, L.; Scrosati, B.; Serraino-Fiory, F.; Plichta, E.; Hendrickson, M. Role of the ceramic fillers in enhancing the transport properties of composite polymer electrolytes. *Electrochim. Acta* **2001**, *46* (16), 2457−2461.
(13) Johansson, P.; Ratner, M. A.; Shriver, D. F. The Influence of Inert Oxide Fillers on Poly(ethylene oxide) and Amorphous Poly(ethylene oxide) Based Polymer Electrolytes †. *J. Phys. Chem. B* **2001**, *105* (37), 9016−9021.
(14) Bruce, P. G.; Scrosati, B.; Tarascon, J.-M. Nanomaterials for rechargeable lithium batteries. *Angew. Chem., Int. Ed.* **2008**, *47* (16), 2930−2946.

DOI: 10.1021/acs.macromol.6b00851
Macromolecules 2016, 49, 5244−5255

(15) Croce, F.; Appetecchi, G. B.; Persi, L.; Scrosati, B. Nanocomposite polymer electrolytes for lithium batteries. *Nature* **1998**, *394* (6692), 456−458.
(16) Bandara, L. R. a. K.; Dissanayake, M. a. K. L.; Mellander, B.-E. Ionic conductivity of plasticized(PEO)-$LiCF_3SO_3$ electrolytes. *Electrochim. Acta* **1998**, *43* (10−11), 1447−1451.
(17) Kim, Y. T.; Smotkin, E. S. The effect of plasticizers on transport and electrochemical properties of PEO-based electrolytes for lithium rechargeable batteries. *Solid State Ionics* **2002**, *149* (1−2), 29−37.
(18) Shin, J. H.; Henderson, W. A.; Passerini, S. Ionic liquids to the rescue? Overcoming the ionic conductivity limitations of polymer electrolytes. *Electrochem. Commun.* **2003**, *5* (12), 1016−1020.
(19) Rhoo, H.-J.; Kim, H.-T.; Park, J.-K.; Hwang, T.-S. Ionic conduction in plasticized blend polymer electrolytes. *Electrochim. Acta* **1997**, *42* (10), 1571−1579.
(20) Ito, Y.; Kanehori, K.; Miyauchi, K.; Kudo, T. Ionic conductivity of electrolytes formed from PEO-$LiCF_3SO_3$ complex low molecular weight poly(ethylene glycol). *J. Mater. Sci.* **1987**, *22* (5), 1845−1849.
(21) Choi, B. K.; Kim, Y. W.; Shin, H. K. Ionic conduction in PEO-PAN blend polymer electrolytes. *Electrochim. Acta* **2000**, *45* (8), 1371−1374.
(22) Michael, M. S.; Jacob, M. M. E.; Prabaharan, S. R. S.; Radhakrishna, S. Enhanced lithium ion transport in PEO-based solid polymer electrolytes employing a novel class of plasticizers. *Solid State Ionics* **1997**, *98* (3−4), 167−174.
(23) Tanaka, R.; Sakurai, M.; Sekiguchi, H.; Mori, H.; Murayama, T.; Ooyama, T. Lithium ion conductivity in polyoxyethylene/polyethylenimine blends. *Electrochim. Acta* **2001**, *46* (10−11), 1709−1715.
(24) Acosta, J. Structural, morphological and electrical characterization of polymer electrolytes based on PEO/PPO blends. *Solid State Ionics* **1996**, *85* (1−4), 85−90.
(25) Khurana, R.; Schaefer, J. L.; Archer, L. A.; Coates, G. W. Suppression of Lithium Dendrite Growth Using Cross-Linked Polyethylene/Poly(ethylene oxide) Electrolytes: A New Approach for Practical Lithium-Metal Polymer Batteries. *J. Am. Chem. Soc.* **2014**, *136* (20), 7395−7402.
(26) Zhang, Z.; Jin, J.; Bautista, F.; Lyons, L.; Shariatzadeh, N.; Sherlock, D.; Amine, K.; West, R. Ion conductive characteristics of cross-linked network polysiloxane-based solid polymer electrolytes. *Solid State Ionics* **2004**, *170* (3−4), 233−238.
(27) Watanabe, M. Polymer electrolytes derived from dendritic polyether macromonomers. *Solid State Ionics* **2002**, *148* (3−4), 399−404.
(28) Redfern, P. C.; Curtiss, L. A. Quantum chemical studies of Li^+ cation binding to polyalkyloxides. *J. Power Sources* **2002**, *110* (2), 401−405.
(29) Watanabe, M.; Nagaoka, K.; Kanba, M.; Shinohara, I. Ionic Conductivity of Polymeric Solid Electrolytes Based on Poly(propylene oxide) or Poly(tetramethylene oxide). *Polym. J.* **1982**, *14* (11), 877−886.
(30) Watanabe, M.; Ikeda, J.; Shinohara, I. Effect of Molecular Weight of Polymeric Solvent on Ion Conductive Behavior in Poly(propylene oxide) Solution of $LiClO_4$. *Polym. J.* **1983**, *15* (1), 65−69.
(31) Nagaoka, K.; Naruse, H.; Shinohara, I.; Watanabe, M. High ionic conductivity in poly(dimethyl siloxane-co-ethylene oxide) dissolving lithium perchlorate. *J. Polym. Sci., Polym. Lett. Ed.* **1984**, *22* (12), 659−663.
(32) Kerr, J. B.; Liu, G.; Curtiss, L. A.; Redfern, P. C. Towards room-temperature performance for lithium−polymer batteries. *Electrochim. Acta* **2003**, *48* (14−16), 2305−2309.
(33) Qiao, J.; Chen, Y.; Baker, G. L. Polymer Electrolytes Based on Unsaturated Ethylene Oxide-Segmented Polymers. *Chem. Mater.* **1999**, *11* (9), 2542−2547.
(34) Buriez, O.; Han, Y. B.; Hou, J.; Kerr, J. B.; Qiao, J.; Sloop, S. E.; Tian, M.; Wang, S. Performance limitations of polymer electrolytes based on ethylene oxide polymers. *J. Power Sources* **2000**, *89* (2), 149−155.
(35) Barteau, K. P.; Wolffs, M.; Lynd, N. A.; Fredrickson, G. H.; Kramer, E. J.; Hawker, C. J. Allyl Glycidyl Ether-Based Polymer Electrolytes for Room Temperature Lithium Batteries. *Macromolecules* **2013**, *46* (22), 8988−8994.
(36) Liu, G. Diffusion coefficients in trimethyleneoxide containing comb branch polymer electrolytes. *Solid State Ionics* **2004**, *175* (1−4), 781−783.
(37) Webb, M. A.; Jung, Y.; Pesko, D. M.; Savoie, B. M.; Yamamoto, U.; Coates, G. W.; Balsara, N. P.; Wang, Z.-G.; Miller, T. F. Systematic Computational and Experimental Investigation of Lithium-Ion Transport Mechanisms in Polyester-Based Polymer Electrolytes. *ACS Cent. Sci.* **2015**, *1* (4), 198−205.
(38) Webb, M. A.; Savoie, B. M.; Wang, Z.-G.; Miller, T. F., III Chemically Specific Dynamic Bond Percolation Model for Ion Transport in Polymer Electrolytes. *Macromolecules* **2015**, *48* (19), 7346−7358.
(39) Sarapas, J. M.; Tew, G. N. Poly(ether−thioethers) by Thiol−Ene Click and Their Oxidized Analogues as Lithium Polymer Electrolytes. *Macromolecules* **2016**, *49* (4), 1154−1162.
(40) Schmidt, B. Catalysis at the Interface of Ruthenium Carbene and Ruthenium Hydride Chemistry: Organometallic Aspects and Applications to Organic Synthesis. *Eur. J. Org. Chem.* **2004**, *2004* (9), 1865−1880.
(41) Teran, A. A.; Tang, M. H.; Mullin, S. A.; Balsara, N. P. Effect of molecular weight on conductivity of polymer electrolytes. *Solid State Ionics* **2011**, *203* (1), 18−21.
(42) Wagener, K. B.; Brzezinska, K. Acyclic diene metathesis (ADMET) polymerization: synthesis of unsaturated polyethers. *Macromolecules* **1991**, *24* (19), 5273−5277.
(43) Wagener, K. B.; Brzezinska, K.; Bauch, C. G. Acyclic diene metathesis (ADMET) polymerization. The preparation of sym-unsaturated polyethers by the use of $Mo(CH\text{-}t\text{-}Bu)(N\text{-}2,6\text{-}C_6H_3\text{-}i\text{-}Pr_2)[OCCH_3(CF_3)_2]_2$ catalyst. *Makromol. Chem., Rapid Commun.* **1992**, *13* (2), 75−81.
(44) Vanommeslaeghe, K.; Hatcher, E.; Acharya, C.; Kundu, S.; Zhong, S.; Shim, J.; Darian, E.; Guvench, O.; Lopes, P.; Vorobyov, I.; et al. CHARMM General Force Field: A Force Field for Drug-Like Molecules Compatible with the CHARMM All-Atom Additive Biological Force Fields. *J. Comput. Chem.* **2010**, *31* (4), 671−690.
(45) Stubbs, J. M.; Potoff, J. J.; Siepmann, J. I. Transferable potentials for phase equilibria. 6. United-atom description for ethers, glycols, ketones, and aldehydes. *J. Phys. Chem. B* **2004**, *108* (45), 17596−17605.
(46) Wu, H.; Wick, C. D. Computational Investigation on the Role of Plasticizers on Ion Conductivity in Poly(ethylene oxide) LiTFSI Electrolytes. *Macromolecules* **2010**, *43* (7), 3502−3510.
(47) Plimpton, S. Fast Parallel Algorithms for Short-Range Molecular-Dynamics. *J. Comput. Phys.* **1995**, *117* (1), 1−19.
(48) Brown, W. M.; Kohlmeyer, A.; Plimpton, S. J.; Tharrington, A. N. Implementing molecular dynamics on hybrid high performance computers - Particle-particle particle-mesh. *Comput. Phys. Commun.* **2012**, *183* (3), 449−459.
(49) Brown, W. M.; Wang, P.; Plimpton, S. J.; Tharrington, A. N. Implementing molecular dynamics on hybrid high performance computers - short range forces. *Comput. Phys. Commun.* **2011**, *182* (4), 898−911.
(50) Figueirido, F.; Del Buono, G. S.; Levy, R. M. On finite-size effects in computer simulations using the Ewald potential. *J. Chem. Phys.* **1995**, *103* (14), 6133.
(51) Maitra, A.; Heuer, A. Cation transport in polymer electrolytes: A microscopic approach. *Phys. Rev. Lett.* **2007**, *98* (22), 227802.
(52) Diddens, D.; Heuer, A.; Borodin, O. Understanding the Lithium Transport within a Rouse-Based Model for a PEO/LiTFSI Polymer Electrolyte. *Macromolecules* **2010**, *43* (4), 2028−2036.
(53) Nitzan, A.; Ratner, M. A. Conduction in Polymers: Dynamic Disorder Transport. *J. Phys. Chem.* **1994**, *98*, 1765−1775.
(54) Mogurampelly, S.; Borodin, O.; Ganesan, V. Computer Simulations of Ion Transport in Polymer Electrolyte Membranes. *Annu. Rev. Chem. Biomol. Eng.* **2016**, *7* (1), 349−371.

DOI: 10.1021/acs.macromol.6b00851
Macromolecules 2016, 49, 5244−5255

(55) Devaux, D.; Bouchet, R.; Glé, D.; Denoyel, R. Mechanism of ion transport in PEO/LiTFSI complexes: Effect of temperature, molecular weight and end groups. *Solid State Ionics* **2012**, *227*, 119−127.
(56) Pesko, D. M.; Jung, Y.; Hasan, A. L.; Webb, M. A.; Coates, G. W.; Miller, T. F.; Balsara, N. P. Effect of monomer structure on ionic conductivity in a systematic set of polyester electrolytes. *Solid State Ionics* **2016**, *289*, 118−124.
(57) Watanabe, M.; Itoh, M.; Sanui, K.; Ogata, N. Carrier transport and generation processes in polymer electrolytes based on poly-(ethylene oxide) networks. *Macromolecules* **1987**, *20* (3), 569−573.
(58) Panday, A.; Mullin, S.; Gomez, E. D.; Wanakule, N.; Chen, V. L.; Hexemer, A.; Pople, J.; Balsara, N. P. Effect of Molecular Weight and Salt Concentration on Conductivity of Block Copolymer Electrolytes. *Macromolecules* **2009**, *42* (13), 4632−4637.
(59) Yuan, R.; Teran, A. A.; Gurevitch, I.; Mullin, S. A.; Wanakule, N. S.; Balsara, N. P. Ionic Conductivity of Low Molecular Weight Block Copolymer Electrolytes. *Macromolecules* **2013**, *46* (3), 914−921.
(60) Chintapalli, M.; Chen, X. C.; Thelen, J. L.; Teran, A. A.; Wang, X.; Garetz, B. A.; Balsara, N. P. Effect of Grain Size on the Ionic Conductivity of a Block Copolymer Electrolyte. *Macromolecules* **2014**, *47* (15), 5424−5431.
(61) Petrowsky, M.; Frech, R. Temperature Dependence of Ion Transport: The Compensated Arrhenius Equation. *J. Phys. Chem. B* **2009**, *113* (17), 5996−6000.
(62) Mullerplathe, F.; Vangunsteren, W. F. Computer-Simulation of a Polymer Electrolyte - Lithium Iodide in Amorphous Poly(Ethylene Oxide). *J. Chem. Phys.* **1995**, *103* (11), 4745−4756.

DOI: 10.1021/acs.macromol.6b00851
Macromolecules 2016, 49, 5244−5255